BRAIN COMMUNICATIONS

Phenotypic assays in yeast and zebrafish reveal drugs that rescue *ATP13A2* deficiency

Ursula Heins-Marroquin,[1] Paul P. Jung,[1] Maria Lorena Cordero-Maldonado,[1] Alexander D. Crawford[1,2,3,*] and Carole L. Linster[1,*]

*These authors contributed equally to this work.

Mutations in *ATP13A2* (*PARK9*) are causally linked to the rare neurodegenerative disorders Kufor-Rakeb syndrome, hereditary spastic paraplegia and neuronal ceroid lipofuscinosis. This suggests that ATP13A2, a lysosomal cation-transporting ATPase, plays a crucial role in neuronal cells. The heterogeneity of the clinical spectrum of *ATP13A2*-associated disorders is not yet well understood and currently, these diseases remain without effective treatment. Interestingly, ATP13A2 is widely conserved among eukaryotes, and the yeast model for *ATP13A2* deficiency was the first to indicate a role in heavy metal homeostasis, which was later confirmed in human cells. In this study, we show that the deletion of *YPK9* (the yeast orthologue of *ATP13A2*) in *Saccharomyces cerevisiae* leads to growth impairment in the presence of Zn^{2+}, Mn^{2+}, Co^{2+} and Ni^{2+}, with the strongest phenotype being observed in the presence of zinc. Using the *ypk9*Δ mutant, we developed a high-throughput growth rescue screen based on the Zn^{2+} sensitivity phenotype. Screening of two libraries of Food and Drug Administration-approved drugs identified 11 compounds that rescued growth. Subsequently, we generated a zebrafish model for *ATP13A2* deficiency and found that both partial and complete loss of *atp13a2* function led to increased sensitivity to Mn^{2+}. Based on this phenotype, we confirmed two of the drugs found in the yeast screen to also exert a rescue effect in zebrafish—*N*-acetylcysteine, a potent antioxidant, and furaltadone, a nitrofuran antibiotic. This study further supports that combining the high-throughput screening capacity of yeast with rapid *in vivo* drug testing in zebrafish can represent an efficient drug repurposing strategy in the context of rare inherited disorders involving conserved genes. This work also deepens the understanding of the role of ATP13A2 in heavy metal detoxification and provides a new *in vivo* model for investigating *ATP13A2* deficiency.

1 Luxembourg Centre for Systems Biomedicine, University of Luxembourg, L-4367 Belvaux, Luxembourg
2 Faculty of Veterinary Medicine, Norwegian University of Life Sciences, 0454 Oslo, Norway
3 Institute for Orphan Drug Discovery, Bremer Innovations- und Technologiezentrum, 28359 Bremen, Germany

Correspondence to: Dr. Carole L. Linster
Luxembourg Centre For Systems Biomedicine
University of Luxembourg, Campus Belval
6 avenue du Swing, L-4367 Belvaux, Luxembourg
E-mail: carole.linster@uni.lu

Keywords: ATP13A2; budding yeast; drug screening; heavy metals; zebrafish

Abbreviations: DMSO = dimethyl sulfoxide; dpf =days post-fertilization; EDTA = ethylenediaminetetraacetic acid; EMA = European Medicines Agency; FDA = Food and Drug Administration; FTD = furaltadone; HTP = high-throughput; KRS = Kufor-Rakeb syndrome; MO = morpholino antisense oligonucleotide; NAC = N-acetylcysteine; OMIM = Online Mendelian Inheritance in Man; PDR5 = pleiotropic drug resistance 5; qPCR = quantitative PCR; TEPA = tetraethylenepentamine

Received March 21, 2019. Revised July 27, 2019. Accepted August 16, 2019. Advance Access publication September 27, 2019

Graphical Abstract

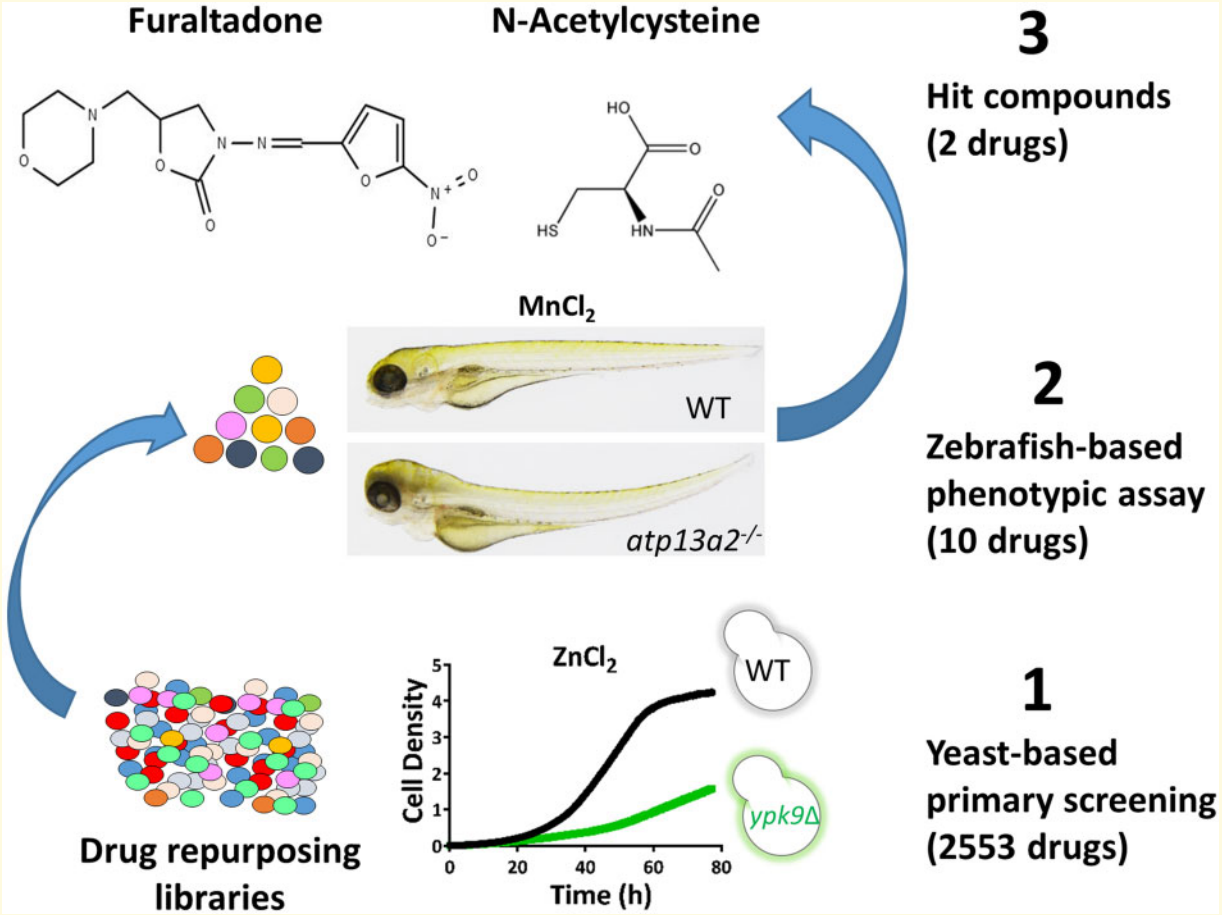

Introduction

ATP13A2, also known as PARK9 or CLN12 (Ramirez *et al.*, 2006; Bras *et al.*, 2012), belongs to the poorly characterized P5-type ATPase family of transport proteins (van Veen *et al.*, 2014). The *ATP13A2* gene encodes a lysosomal and late endosomal transmembrane protein of 1180 amino acids involved in cation transport, whose precise molecular function remains unknown. *ATP13A2* is widely expressed by many neuronal populations, and more particularly in the dopaminergic neurons of the substantia nigra (Schultheis *et al.*, 2004; Ramirez *et al.*, 2006). Recessive mutations in the *ATP13A2* gene were initially described to cause Kufor-Rakeb syndrome (KRS; OMIM# 606693), an atypical juvenile Parkinsonism with dementia and progressive brain atrophy (Ramirez *et al.*, 2006). However, with the advent of new sequencing technologies and bioinformatics tools, the genetic and clinical spectra of *ATP13A2* deficiencies have been expanded. Namely, *ATP13A2* mutations have been additionally causally associated with a juvenile form of neuronal ceroid lipofuscinosis (OMIM# 606693; Farias *et al.*, 2011; Bras *et al.*, 2012) and a complicated form of hereditary spastic paraplegia-78 (OMIM# 617225; Kara *et al.*, 2016; Estrada-Cuzcano *et al.*, 2017). Juvenile neuronal ceroid lipofuscinosis is classified as a fatal lysosomal storage disorder characterized by the accumulation of an autofluorescent hydrophobic material called lipofuscin (Palmer *et al.*, 1992). In contrast, hereditary spastic paraplegia-78 is considered as an adult neurodegenerative disorder, in which a main clinical feature is the progressive spasticity of the lower limbs due to axonopathy of the corticospinal neurons (Estrada-Cuzcano *et al.*, 2017). Even more recently, the phenotypic spectrum associated with variants in the *ATP13A2* gene was further expanded to also include a juvenile-onset form of amyotrophic lateral sclerosis (Spataro *et al.*, 2019).

Although these four neurodegenerative diseases differ substantially from a clinical point of view, the cellular phenotypes associated with *ATP13A2* deficiency converge. Studies in fibroblasts derived from KRS and hereditary spastic paraplegia-78 patients showed similar lysosomal and mitochondrial dysfunction phenotypes (Grunewald *et al.*, 2012; Usenovic *et al.*, 2012*b*; Estrada-Cuzcano *et al.*, 2017). Furthermore, animal models of juvenile neuronal ceroid lipofuscinosis and KRS both

featured age-related motor dysfunction, protein aggregation and lipofuscinosis (Farias *et al.*, 2011; Wohlke *et al.*, 2011; Schultheis *et al.*, 2013; Kett *et al.*, 2015). Interestingly, the *ATP13A2* p.(T512I) missense variant has been described in patients diagnosed with KRS and hereditary spastic paraplegia-78, suggesting that environmental factors can determine the development of the clinical phenotype (Dehay *et al.*, 2012; Usenovic *et al.*, 2012*a*; Estrada-Cuzcano *et al.*, 2017).

In fact, *ATP13A2* polymorphisms have been identified in one study as potential risk markers for neurotoxic effects of manganese in humans and two KRS patients have been reported so far with increased iron levels in the brain (Behrens *et al.*, 2010; Schneider *et al.*, 2010; Rentschler *et al.*, 2012). These two metals are currently the major metals associated with secondary Parkinsonism and increasing evidence suggests that heavy metal exposure is involved in several neurodegenerative conditions (Grubman *et al.*, 2014; Cicero *et al.*, 2017). Interestingly, the deletion of *YPK9* (yeast orthologue of *ATP13A2*) in *Saccharomyces cerevisiae* led to decreased resistance against heavy metal toxicity (Gitler *et al.*, 2009; Schmidt *et al.*, 2009). The link between ATP13A2 and heavy metal homeostasis has received further support by subsequent studies in various mammalian cell models (Tan *et al.*, 2011; Kong *et al.*, 2014; Park *et al.*, 2014).

Despite the strong evidence for a role of ATP13A2 in heavy metal homeostasis, the precise function of ATP13A2 remains unclear and there is currently no effective treatment to cure or reverse the symptoms of any of the *ATP13A2*-associated disorders. Others have previously shown that a 2-step phenotypic drug-screening approach in a more simple followed by a more complex model organism can be a promising strategy to identify potential lead compounds for inherited human disorders (Cotticelli *et al.*, 2012; Soma *et al.*, 2018; Vincent *et al.*, 2018). Similarly, we took advantage of the apparent functional conservation of *ATP13A2* across species to develop a drug-screening pipeline combining yeast (*S. cerevisiae*) and zebrafish (*Danio rerio*) models of *ATP13A2* deficiency. Rapid growth, low cultivation costs and good reproducibility make budding yeast an excellent eukaryotic cell model for performing high-throughput (HTP) primary drug screens. HTP phenotypic screens in yeast models have, for instance, revealed compounds protecting against types of proteotoxicity relevant for human neurodegenerative disorders (Tardiff *et al.*, 2012, 2013; Vincent *et al.*, 2018). In this study, we screened >2500 compounds, including many approved drugs, for their ability to rescue growth in yeast *ypk9*Δ strains in the presence of toxic levels of zinc. Eleven validated hits were further tested for their ability to rescue a decreased manganese resistance phenotype identified in *atp13a2* deficient zebrafish larvae. As an outcome, *N*-acetylcysteine (NAC) and furaltadone (FTD), a nitrofuran antibiotic, emerged as compounds that actively protect against increased metal sensitivity induced by *ATP13A2* deficiency, in both yeast and zebrafish models. More generally, our study further supports that coupling large-scale primary drug screening in yeast followed by a more focused validation screen in the whole-organism zebrafish model represents a powerful approach to discover lead compounds for inherited human disorders involving conserved disease genes.

Materials and methods

Yeast strains

*ypk9*Δ strains were generated in the BY4742 and FY4 backgrounds. The BY4742*ypk9*Δ strain was obtained by crossing the BY4741*ypk9*Δ strain from the gene deletion collection (EUROSCARF) with wild-type (WT) BY4742, followed by tetrad dissection to isolate the genotype of interest. The FY4*ypk9*Δ strain was created via PCR-mediated gene replacement by the kanMX4 cassette (Brachmann *et al.*, 1998) in the FY4 parental strain, which was a kind gift from Joseph Schacherer. To generate rescue strains, the *YPK9* gene was amplified from yeast genomic DNA and cloned into the pAG303GPD-ccdB plasmid using Gateway technology (Alberti *et al.*, 2007). Both the recombinant and empty plasmids were integrated into the *HIS3* locus of BY4742*ypk9*Δ cells and positive clones were selected on synthetic complete medium lacking histidine. To generate the *ypk9*Δ*pdr5*Δ double mutant, the *PDR5* gene was replaced by the *URA3* marker in the BY4742*ypk9*Δ strain, followed by selection on synthetic complete medium lacking uracil. Transformations were performed using a standard polyethylene glycol/lithium acetate protocol as previously described (Gietz and Woods, 2002), and correct gene disruption or gene integration was verified by PCR. The strains, plasmids and primers used in this study are listed in Supplementary Tables 1–3.

Yeast cultivation media and growth conditions

Rich media (YPD) used for yeast transformation experiments contained 10 g/l yeast extract, 20 g/l peptone and 20 g/l glucose. For all other cultivations in this study (metal ion measurements, growth phenotyping and drug screening), yeast cells were grown in YNB (6.7 g/l yeast nitrogen base without amino acids, 5 g/l ammonium sulfate, pH 5) supplemented with 20 g/l glucose, 0.08 g/l histidine, uracil, methionine, lysine and 0.24 g/l leucine. When needed for selection, the media were supplemented with geneticin (200 µg/ml). Metal solutions were sterilized by filtration and added at indicated concentrations to YNB medium.

Growth phenotyping assay in yeast

Yeast growth phenotyping was performed as previously described (Jung *et al.*, 2015). Growth rate, final biomass

and lag time were analysed using the GATHODE software (Jung *et al.*, 2015). The growth conditions tested in this study are listed in Supplementary Table 4.

Drug screening in yeast

Two fresh single colonies of the *ypk9Δpdr5Δ* strain were inoculated from solid YPD plates into 5 ml YNB media with specific supplementation (as described above) and incubated overnight with shaking (200 rpm) at 30°C. After 16 h, 400 µl of overnight culture was inoculated into 4 ml fresh media and cultivated until the optical density at 600 nm (OD_{600}) reached about 0.5. Compound plates were prepared by dispensing 25 µl growth media containing 15 mM $ZnCl_2$ into sterile 384-well microplates using an electronic 384-channel VIAFLO pipette (INTEGRA). 0.05 and 0.5 µl droplets of 10 mM drug stock solutions in dimethyl sulfoxide (DMSO) were added using an ECHO550 contactless acoustic nanolitre dispensing system (Labcyte). The first and last two columns of each test plate were reserved for various controls. Finally, 25 µl of cell suspension diluted to a starting OD_{600} of about 0.0125 in growth medium supplemented with 15 mM $ZnCl_2$ were added to each well. Positive, negative, viability and contamination control wells contained 4.5 mM EDTA, 1% or 0.1% DMSO instead of drug solution, water instead of $ZnCl_2$ and water instead of cell inoculate, respectively. Microplates were incubated at 30°C and OD_{600} measurements were recorded using a TECAN M200 plate reader just after the inoculation of the cells as well as 48 h and 96 h later. The screening was performed as a biological duplicate, meaning that each drug was tested twice in two independent experiments. The statistical methods applied to the drug-screening data for quality assessment and hit identification are described in the Supplementary material.

Metal ion measurements by inductively coupled plasma—mass spectrometry

Intracellular Zn^{2+} concentrations were measured by inductively coupled plasma—mass spectrometry (Agilent 7900) in samples prepared from three independent yeast cultivations as described in the Supplementary material.

Zinquin chelation assay

A solution of 20 µM Zinquin (Sigma-Aldrich) was mixed with 5, 10, 25 and 50 µM of selected drugs with or without 5 µM $ZnCl_2$ in phosphate-buffered saline at pH 7.0. Mixtures were incubated for 1 h at 25°C and shaking at 300 rpm. The samples were then transferred into a 96-well plate for fluorescence measurements in a microplate reader, at an excitation wavelength of 370 nm and an emission wavelength of 490 nm. Three independent replicates were measured per condition tested. The fluorescence intensities of the $ZnCl_2$-containing samples were background-corrected by subtracting the fluorescence intensity of the corresponding samples incubated in the absence of $ZnCl_2$.

Zebrafish strains

The *atp13a2*$^{sa18624+/-}$ and *atp13a2*$^{sa14250+/-}$ zebrafish lines (TLF background, F3 generation) were obtained from the European Zebrafish Resource Center and kept in our aquatic facility according to standard protocols (Westerfield, 2000). These *atp13a2* lines were further outcrossed with WT (AB) or *nacre* lines.

Zebrafish embryos were obtained by natural spawning and then incubated in the dark at 28°C, in Danieau's solution [17 mM NaCl, 2 mM KCl, 0.12 mM $MgSO_4$, 1.8 mM $Ca(NO_3)_2$, 1.5 mM HEPES pH 7.5 and 1.2 µM methylene blue]. If needed, to inhibit pigmentation, 24 h post-fertilization embryos were incubated in Danieau's solution with 0.2 mM 1-phenyl-2-thiourea (PTU, Sigma). For live imaging, larvae were anaesthetized with buffered MS222 (0.016% w/v).

Ethics statement concerning zebrafish manipulations

The Aquatic Facility at the Luxembourg Centre for Systems Biomedicine is registered as an authorized breeder, supplier and user of zebrafish with Gran-Ducal decree of 20 January 2016. All practices involving zebrafish were performed in accordance with European laws, guidelines and policies for animal experimentation, housing and care (European Directive 2010/63/EU on the protection of animals used for scientific purposes). Authorization number LUPA 2017/04 allowed the performance of fin biopsies for genotyping purposes. Besides this, the present study did not involve any additional procedures within the meaning of Article 3 of Directive 2010/63/EU and as such it was not subjected to authorization by an ethics committee.

Genotyping of zebrafish lines

The *atp13a2*^{sa18624} and *atp13a2*^{sa14250} lines were fin-clipped and genotyped by PCR followed by AluI restriction analysis or sequencing, respectively. Detailed protocols and primer sequences are given in the Supplementary material and Supplementary Table 3.

Gene knockdown in zebrafish using morpholino antisense oligonucleotides

Translation and splice-blocking morpholinos (MOs) for *atp13a2* and non-targeting control MOs were purchased from Gene Tools. Manual microinjections of MOs were performed as previously described (Rosen *et al.*, 2009).

Morpholino sequences and the microinjection procedure are provided in the Supplementary material.

RNA extraction and quantitative PCR to study the tissular distribution of zebrafish *atp13a2*

Gene expression was analysed by quantitative PCR (qPCR) using the LightCycler480 (Roche). For each tissue, qPCR reactions were run for three biological replicates and two technical replicates were performed for each qPCR reaction. Expression levels of *atp13a2* in indicated tissues were calculated relative to the eye tissue using the $2^{-\triangle\triangle Ct}$ method (Livak and Schmittgen, 2001). *ef1α* and *rpl13α* were used as reference genes for normalization. Tissular RNA extraction and cDNA synthesis protocols are detailed in the Supplementary material and the qPCR primer sequences are listed in Supplementary Table 3.

Heavy metal toxicity assay and drug screening in zebrafish

Two days post-fertilization (dpf) *atp13a2*$^{-/-}$ mutant embryos or *atp13a2* knockdown morphants were incubated in a 48-well plate with Danieau's solution containing varying concentrations of $MnCl_2$. The Mn^{2+}-containing solution was renewed after 24 h and the toxicity assessed at 5 dpf. Experiments were performed with 12 larvae per well in quadruplet ($n = 48$) for each tested condition. For the drug screening, a similar procedure was applied but with drugs or vehicle (DMSO or water) added at 3 dpf and here experiments were performed with 12 or 15 larvae per well in triplicate. For consistency in the phenotypic scoring, all the experiments were performed by a single person, but the final hit confirmation for NAC and FTD in zebrafish was performed in 'single-blinded' experiments, in which the experimentalist did not know which larvae received which treatment, to avoid biased results.

Statistical analysis

All data are presented as means ± standard deviations (SDs). The statistical tests used for data analysis are described in the corresponding figure legends. Two-way ANOVA analyses with the respective *post hoc* tests were performed using the GraphPad Prism software (version 8.2.0) and extended statistics for the ANOVA tests are provided in Supplementary Table 5. The likelihood ratios for the zebrafish experiments were calculated using RStudio (version 1.0.143).

Data availability

The authors confirm that the data supporting the findings of this study are nearly fully available within the article and its supplementary documents. Additional supporting data are available from the corresponding author upon request.

Results

Deletion of the *ATP13A2* homologue in yeast triggers metal hypersensitivity

Under standard yeast cultivation conditions, *ypk9*Δ strains grew similarly to WT control strains. In order to identify a phenotype suitable for implementing an HTP drug screen under *YPK9* deficiency, we assayed the growth of WT and *ypk9*Δ strains in >200 different conditions in liquid microcultivation (Supplementary Table 4). For a subset of the growth conditions, including different carbon sources, pH values, stressors, drugs and defined concentrations of various heavy metals, we tested WT and knockout strains in two different genetic backgrounds (BY4742 and FY4) and additionally a *YPK9* rescue strain (*YPK9*$_{OE}$) in the BY4742 background (Fig. 1A and Supplementary Table 4). In both backgrounds, *YPK9* deficiency led to a slowed growth phenotype only in the presence of certain metals (Zn^{2+}, Mn^{2+}, Ni^{2+} and Co^{2+}, but not Ca^{2+}, Li^{+} and Cu^{2+}) in the cultivation medium. Although we were not able to detect a previously reported growth defect of the *ypk9*Δ strain in the presence of Cd^{2+} (Schmidt *et al.*, 2009), we found that overexpression of *YPK9* enhanced growth under Cd^{2+}exposure (Fig. 1A). Subsequently, high-density growth curves (allowing for specific growth rate and yield of biomass calculation) were determined in the presence of the divalent metals Zn^{2+}, Mn^{2+}, Ni^{2+} and Co^{2+} for the WT, *ypk9*Δ and *YPK9*$_{OE}$ strains (BY4742 background), at concentrations that we had previously shown to significantly impair the growth of *ypk9*Δ cells (Supplementary Fig. 1A and Fig. 1B). Overexpression of *YPK9* in the *ypk9*Δ strain rescued the growth defects induced by the metal ion exposures, supporting that these phenotypes were gene-specific (Fig. 1B). These results fully support that Ypk9, as previously suggested by others, is mainly involved in metal homeostasis (Gitler *et al.*, 2009; Schmidt *et al.*, 2009) and shed some light on the specificity of this effect.

Zn^{2+}, Ni^{2+} and Co^{2+} induced strong growth impairments in the *ypk9*Δ strain, as reflected in both the yield of biomass (60–80% lower compared with the WT strain) and in the growth rate (38–50% lower than WT; Fig. 1C). In contrast, Mn^{2+} decreased the growth rate of the *ypk9*Δ strain without significantly affecting the biomass. As Zn^{2+} is physiologically more relevant than Ni^{2+} and Co^{2+}, we were interested to test the effect of *YPK9* deficiency on intracellular Zn^{2+} pools. In the absence of supplemented zinc, the WT, *ypk9*Δ and *YPK9*$_{OE}$ strains

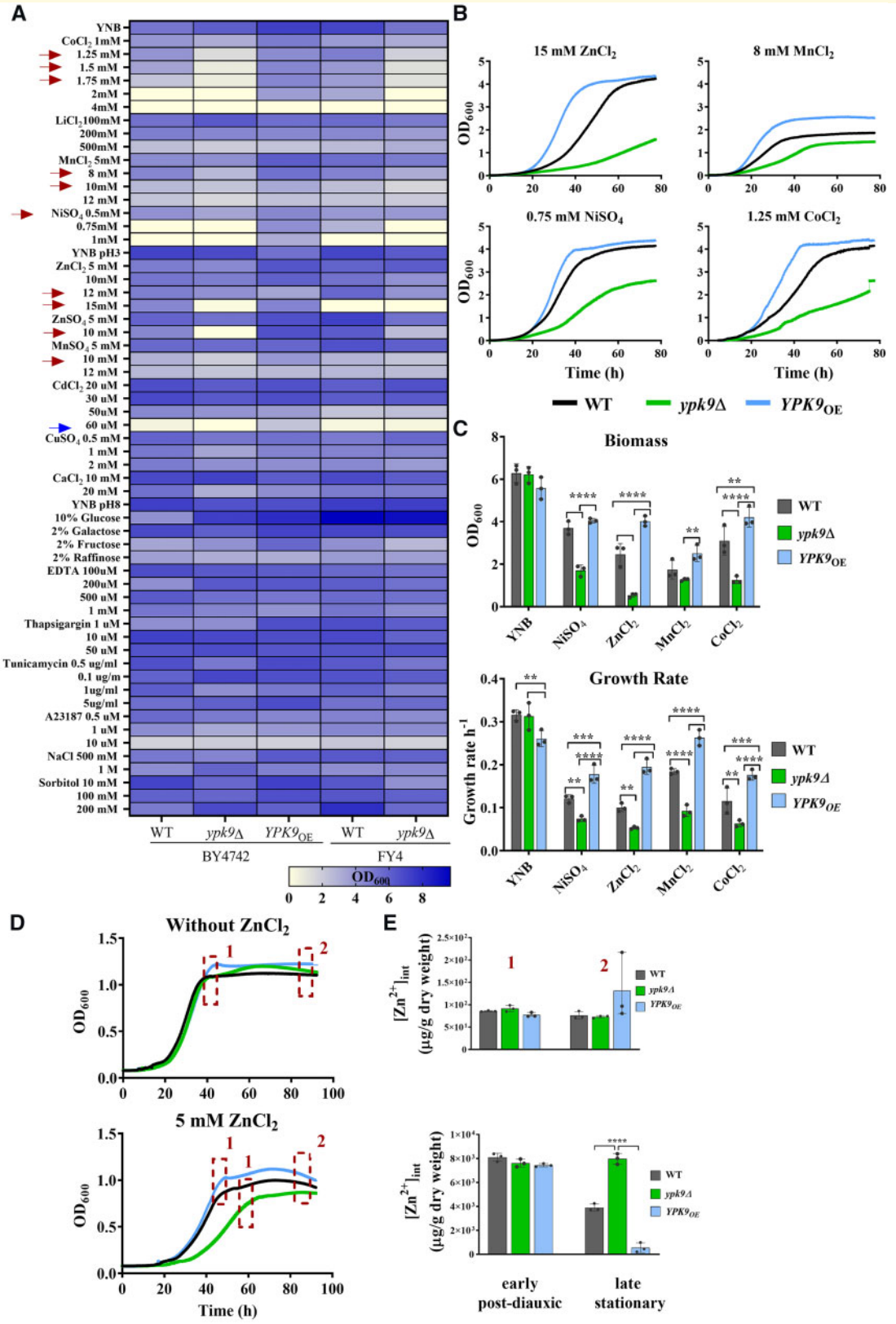

Figure 1 Large-scale phenotyping of *ypk9*Δ strains and validation of growth conditions for drug screening. (**A**) Heat map representing OD_{600} values measured 48 h after the inoculation of liquid microcultures in the indicated conditions with WT, *ypk9*Δ and *YPK9* overexpression ($YPK9_{OE}$) strains (BY4742 and/or FY4 background). The deletion of *YPK9* resulted in growth defects in media containing Co^{2+}, Mn^{2+}, Zn^{2+} and Ni^{2+} (red arrows) and *YPK9* overexpression rescued the growth defects (red and blue arrows). (**B**) Representative growth curves of WT, *ypk9*Δ and $YPK9_{OE}$ strains (BY4742 background) obtained in an independent experiment in the presence of Zn^{2+}, Mn^{2+}, Ni^{2+} and Co^{2+} at the indicated concentrations. (**C**) Biomass (at 48 h) and growth rates determined from the growth curves shown in **B**. (**D**) Growth curves of the same strains in minimal growth medium supplemented or not with 5 mM $ZnCl_2$. Red boxes indicate the sampling points for metal

showed similar intracellular Zn^{2+} concentrations (≈80–90 µg/g dry weight) at the two measurement time points (early post-diauxic and stationary phase; Fig. 1D and E). Supplementation of 5 mM $ZnCl_2$ increased the intracellular Zn^{2+} concentrations about 100 times (≈7000–8000 µg/g dry weight). Interestingly, WT cells, but not *ypk9*Δ cells, were able to reduce the intracellular Zn^{2+} levels by about 2-fold; this decrease was even more drastic (14-fold) when *YPK9* was overexpressed (Fig. 1E). These results suggest that *YPK9* is not essential for cell proliferation in the presence of subtoxic levels of Zn^{2+}, but that it plays an important role in the stress response induced by overexposure to this and probably some other metals in post-mitotic and/or aged cells. The observation that *YPK9* overexpression led to intracellular Zn^{2+} levels that are lower than in the WT strain is consistent with the growth assays under divalent metal overexposure, where *YPK9* overexpression enhanced growth rate and yield of biomass beyond the WT parameters (Fig. 1B and C), indicating that basal *YPK9* expression levels do not provide optimal protection against metal ion stress.

High-throughput compound screen in an *ATP13A2*-deficient yeast model

HTP drug screening in the yeast model was performed in the 384-well microplate format where cells were cultivated in the presence of 15 mM $ZnCl_2$ at 30°C, with OD_{600} measurements being taken just after inoculation as well as 48 h and 96 h later. To increase the probability of positive hits in the presence of lower drug concentrations, we additionally deleted the *PDR5* gene in our *ypk9*Δ strain. *PDR5* encodes the most pleiotropic drug export pump in budding yeast and its deletion has been shown to increase the susceptibility to externally added compounds (Rogers *et al.*, 2001). We confirmed that *PDR5* deletion did not cause any additional growth impairment in standard conditions or in the presence of $ZnCl_2$, be it in the WT or in the *ypk9*Δ background (Supplementary Fig. 1B). For assay quality assessment, the Z′-factor was calculated for each tested plate based on negative and positive control wells containing DMSO and EDTA, respectively. EDTA restores WT growth by extracellular zinc chelation (Supplementary Fig. 1C) and, given the absence of any currently known drug to treat *ATP13A2* deficiencies, served as a reference point for hit identification. In addition, cell vitality was tested in control wells containing medium devoid of Zn^{2+} and each plate also contained microbial contamination control wells (Fig. 2A).

To identify lead compounds with potential therapeutic value for *ATP13A2* deficiencies, the Prestwick and Tocris chemical libraries, which contain 1280 and 1273 compounds, respectively (of which 815 and 160 correspond to FDA/EMA-approved drugs), were screened using the yeast growth rescue assay. In total, 117 compounds are contained in both libraries and were thus tested twice. In total, 2553 compounds (of which 2436 unique compounds) were tested in duplicate and at two different concentrations (10 and 100 µM). In total, 24 compounds were identified as positive hits in both replicates (Fig. 2B and Supplementary Fig. 2 and Table 6). Of these, 17 compounds tested positive at one concentration only and seven compounds were positive at both concentrations. Of the 24 hit compounds, 22 compounds were re-tested (only three of the five cephalosporin antibiotic hits were further tested so far) and 11 could be validated by showing a reproducible protective effect against Zn^{2+}-induced toxicity in a dose-response assay in the *ypk9*Δ*pdr5*Δ strain, resulting in a validated hit rate of 0.5% (Fig. 2C). These 11 compounds can be grouped into three categories: (i) non-FDA-approved drugs (VU152100, VU10010, ML-365 and AMG-9810), (ii) antibiotics (moxalactam, cefmetazole, cefazolin and FTD) and (iii) direct or indirect chelators [NAC, deferoxamine and tetraethylenepentamine (TEPA)].

As seen in Fig. 2C, all validated drugs slightly alleviated the Zn^{2+}-induced stress in WT cells, at least at the lower concentrations tested. In contrast, a stronger and dose-dependent positive effect was observed in *YPK9* deficient cells. With the non-FDA-/EMA-approved compounds, virtually full rescue effects were reached at relatively low concentrations. These drugs precipitated at higher concentrations (>300 µM) and were, therefore, not tested at higher doses. Moreover, foam formation in microcultivations containing AMG9810 interfered with the OD measurements, leading to high variations in the results obtained with this compound. The remaining (FDA-approved) drugs were more soluble in water and were tested at higher concentrations without toxic effect, except for two antibiotics (FTD and cefazolin) that impaired growth of both WT and *YPK9* deficient cells at the higher doses tested. Within the antibiotic group, containing cephalosporin antibiotics from different generations, cefmetazole exerted the strongest rescue effect. In the chelator group, a nearly full rescue effect was reached with NAC and TEPA, whereas only a moderate effect was observed with the lower concentrations tested for deferoxamine.

ion analysis (1: early post-diauxic phase; 2: late stationary phase). (**E**) Intracellular Zn^{2+} concentrations measured by inductively coupled plasma—mass spectrometry in the indicated strains at the indicated growth phases. During the late stationary phase, WT and $YPK9_{OE}$ were able to significantly reduce the intracellular concentration compared to the early post-diauxic phase. In contrast, Δ*ypk9* showed similar Zn levels, suggesting that Zn compartmentalization/externalization is affected in these cells. In **C** and **E**, values shown are means ± SDs of three biological replicates. Statistically significant differences between strains were determined using the two-way ANOVA test followed by Tukey's multiple comparisons test (**$P < 0.01$, ***$P < 0.001$, ****$P < 0.0001$).

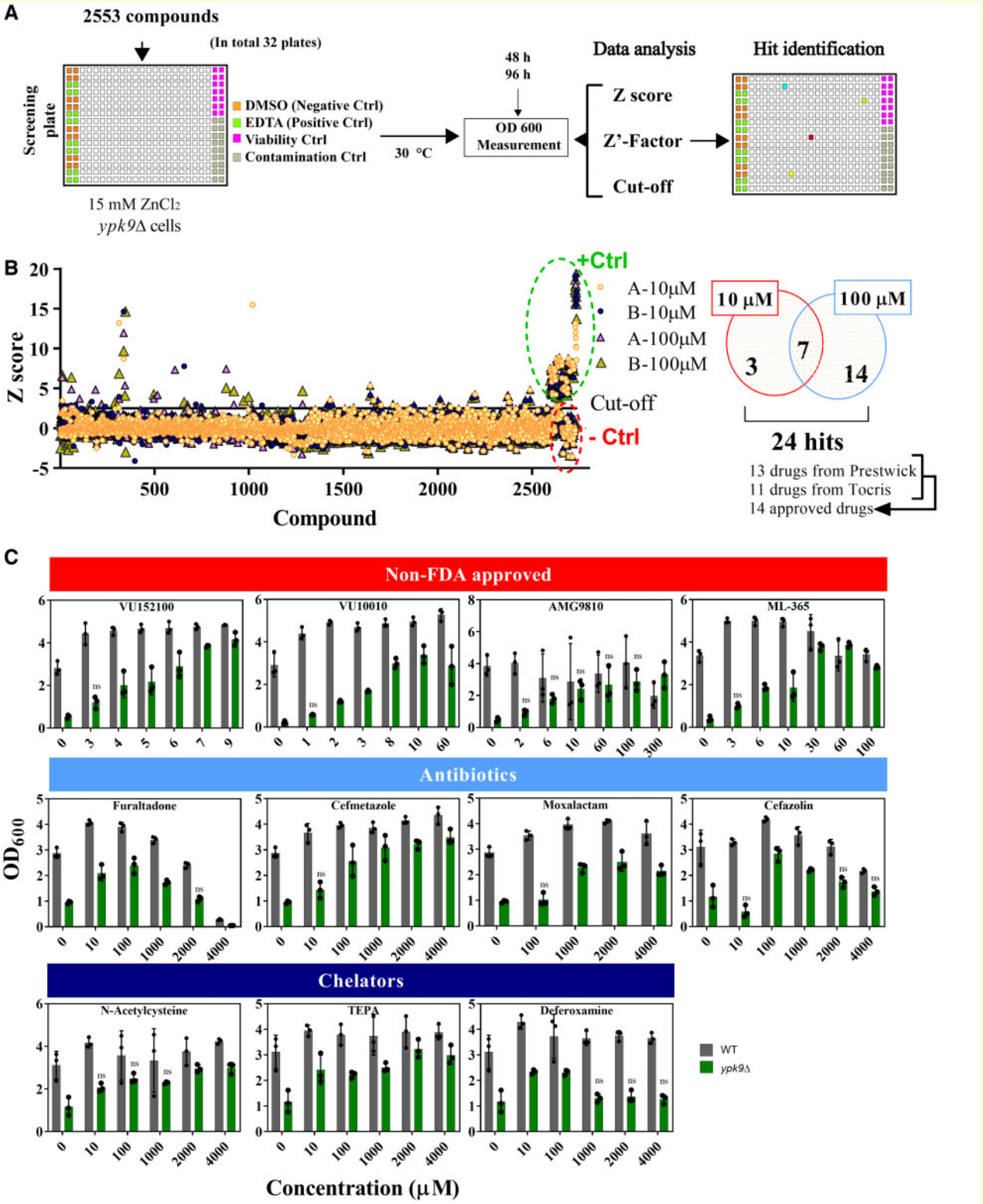

Figure 2 Drug screening of the Prestwick and Tocris chemical libraries in a yeast *ATP13A2* deficiency model. (**A**) Pipeline for drug screening in 384-well plate format. Positive controls (4.5 mM EDTA, $n = 16$) and negative controls (0.1 and 1% DMSO, $n = 16$) were alternated in the first and second columns of each plate. The last two columns of each plate were reserved for 16 vitality (no metal) and 16 contamination (no cell inoculation) control wells. Drugs ($n = 2553$) were tested at 10 and 100 μM in biological duplicates. OD_{600} was measured 48 and 96 h after inoculation and standard statistical analysis for HTP drug-screening data was performed for each time point in order to determine the indicated parameters. (**B**) *Z*-scores for the screening plates with acceptable *Z'*-factor. From both libraries, 24 drugs were identified as positive hits (*Z*-score > cut-off value). Of those, 10 drugs were positive at 10 μM, 21 drugs at 100 μM and 14 were FDA-approved drugs. (**C**) From the 24 hits, 11 were validated in independent dose-response assays. Data shown are means ± SDs for three biological replicates. Statistically significant

Chelation activity of the yeast phenotypic hit compounds

The discrepancy between the concentrations at which the yeast phenotypic hit compounds at least started to exert rescue effects (10–100 μM) and the $ZnCl_2$ concentration present in the cultivation medium (15 mM) for the drug-screening and dose-response assays suggested that the main mechanism of action of the hit compounds was not extracellular metal ion chelation. To consolidate this assumption, a fluorometric chelation assay using zinquin was performed to assess the chelation activity of the hit compounds. Zinquin forms a fluorescent complex with Zn^{2+} ions and the complex is UV-excitable. As positive controls, we used EDTA and clioquinol, both well-known Zn^{2+} chelators. The strong chelator EDTA completely sequestered the Zn^{2+} (20 μM) bound to zinquin already at the lowest concentration tested (10 μM), whereas clioquinol showed an increasing chelation activity between 5 and 50 μM. Except for VU152100 and VU10010 (which interfered with the zinquin chelation assay, due to their strong inherent fluorescence), the chelation activity of all the validated yeast phenotypic hit compounds was assessed in this same concentration range (Fig. 3A). Only TEPA, an industrial iron chelator, showed a relatively strong Zn^{2+} chelation activity, comparable with clioquinol at the highest concentration tested. From the eight remaining compounds, only the nitrofuran antibiotic FTD displayed also a dose-dependent, but much more moderate chelation activity (Fig. 3A). These results thus strongly suggest that our positive hits, except perhaps for TEPA, did not simply rescue the zinc sensitivity phenotype by 'sweeping up' the zinc added extracellularly to challenge our yeast model, but rather acted intracellularly to compensate more or less fully for the *ATP13A2* deficiency.

atp13a2 loss-of-function leads to decreased resistance against manganese toxicity in zebrafish

As *ATP13A2*-related disorders will predictably respond mostly to drugs which are able to reach their target site within the central nervous system, we established an *atp13a2* deficient zebrafish model to further validate our positive hit compounds *in vivo*. As the ATP13A2 protein, which shares 50% amino acid sequence identity between human and zebrafish, has been studied only very little in the latter model (Lopes da Fonseca *et al.*, 2013; Spataro *et al.*, 2019), we first analysed the tissue distribution of the *atp13a2* transcript in adult fish using qPCR. *atp13a2* showed the highest expression in both female and male animals in the gonads, the brain and the eyes (Supplementary Fig. 3), further supporting the potential relevance of zebrafish in *ATP13A2*-linked disease modelling. It should be noted that *rpl13α* is more stably expressed across tissues in both males and females than *ef1α* ; therefore, we believe that the relative gene expression results based on the *rpl13α* reference gene are more reliable (McCurley and Callard, 2008; Xu *et al.*, 2016).

Zebrafish lines carrying *atp13a2* mutant alleles (*atp13a2*^{sa14250} or *atp13a2*^{sa18624}) generated by *N*-ethyl-*N*-nitrosourea mutagenesis (Howe *et al.*, 2013) were obtained from the European Zebrafish Resource Center. Each allele carries a single non-sense mutation (2153 T > A or 2457 T > G) resulting in a premature stop codon in exon 20 or exon 22, respectively (Fig. 4A). Both mutations can be predicted to cause a loss-of-function, as they lead to the elimination of important sequences of the P-domain, responsible for the binding of the Mg^{2+}-ATP complex via Mg^{2+} coordination, as well of the transmembrane domains M5-M10 (Sorensen *et al.*, 2010; Fig. 4A). The point mutation in the *atp13a2*^{sa18624} allele creates a new AluI restriction site, allowing to easily follow its transmission through generations by genotyping (Fig. 4B). We, therefore, focused on the *atp13a2*$^{sa18624+/-}$ line, which was backcrossed to a WT line to reduce unspecific mutations generated by *N*-ethyl-*N*-nitrosourea mutagenesis. Heterozygotes of the F5 generation were mated and their offspring ($n = 37$) were genotyped after 2 months; 35% of the progeny was found to be homozygous for the mutation, showing that *atp13a2* deletion in zebrafish is not lethal during development (Fig. 4B). Furthermore, homozygous mutants were able to reach adulthood without any obvious morphological or behavioural abnormalities.

As ATP13A2 seems to play an important role in heavy metal homeostasis (this study; Tan *et al.*, 2011; Park *et al.*, 2014), we tested the effect of manganese on *atp13a2*$^{sa18624+/+}$, *atp13a2*$^{sa18624-/+}$ and *atp13a2*$^{sa18624-/-}$ larvae. Exposure to $MnCl_2$ has previously been described to cause neurodegeneration in zebrafish, and in humans, it leads to manganism, a disorder featuring symptoms that resemble those of Parkinson's diseases (Bakthavatsalam *et al.*, 2014; Roth, 2014). In this study, we exposed zebrafish larvae to 2 and 3 mM $MnCl_2$ and compared the morphological abnormalities at 5 dpf. In the presence of Mn^{2+}, WT and heterozygous larvae showed a moderate phenotype characterized mainly by an underdeveloped swimming bladder. In contrast, homozygous *atp13a2* mutants were highly sensitive to Mn^{2+} and displayed multiple abnormalities, including pericardial oedemas, movement loss and spine curvature in addition to the underdevelopment of the swimming bladder

differences between treated and non-treated *ypk9*Δ cells were determined by the two-way ANOVA test followed by Dunnet's multiple comparison *post hoc* test. Except when otherwise indicated (ns = not significant), the drug concentrations tested had significant effects ($P < 0.01$). WT, *pdr5*Δ strain; KO, *ypk9*Δ*pdr5*Δ strain.

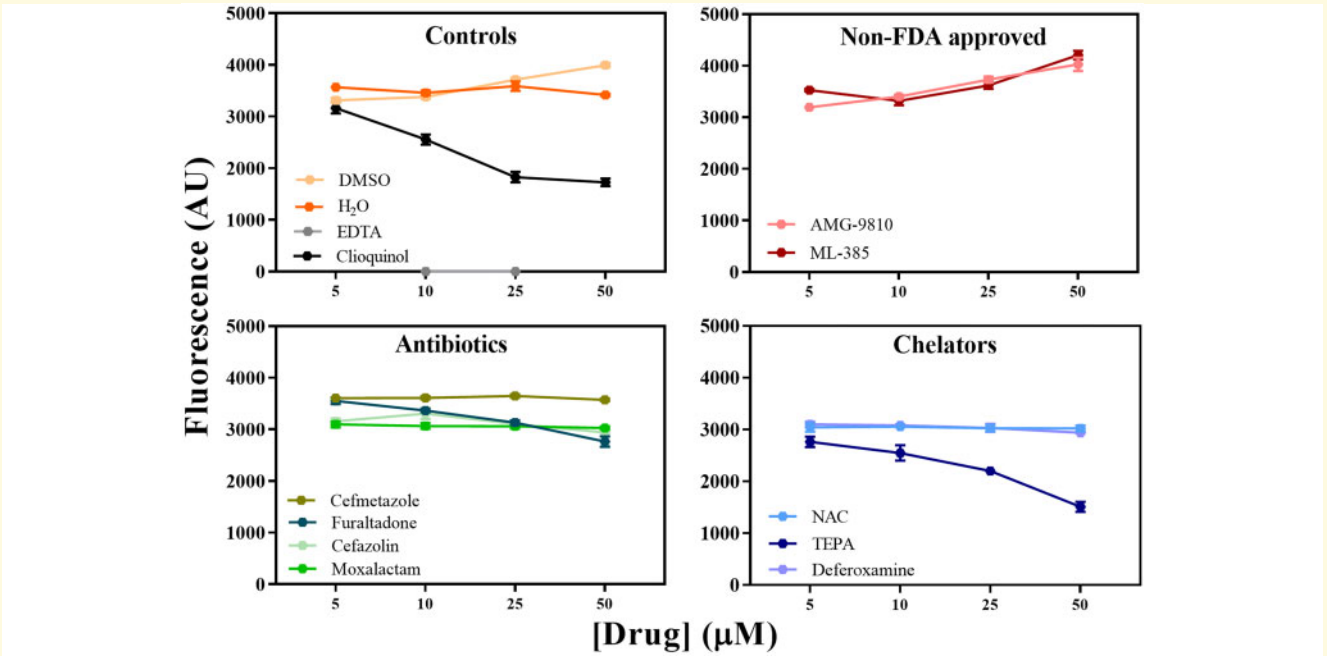

Figure 3 Chelation activity of validated yeast phenotypic rescue compounds. (**A**) Chelation activity was measured based on the Zn^{2+}-selective fluorescent probe zinquin. Background corrected fluorescence intensities (excitation at 370 nm and emission at 490 nm) measured at the indicated drug concentrations are shown. H_2O and DMSO were used as negative controls, EDTA and clioquinol as positive controls. Fluorescence intensities are negatively correlated with Zn^{2+} chelation activity. Data shown are means ± SDs for three independent replicates. AU, arbitrary units.

(Fig. 4C and Supplementary Fig. 4). The homozygous mutant larvae also frequently featured darkening of the brain region, suggesting that this organ might be particularly affected by Mn^{2+} exposure in the absence of functional ATP13A2. Similar results were obtained in the second mutant line (*atp13a2*^{sa14250}) upon exposure to Mn^{2+} (Supplementary Fig. 5). To uncover possible reasons for the darkening of the brain in mutant *atp13a2*$^{sa18624-/-}$ larvae, a TUNEL assay was performed in 5 dpf larvae exposed or not to Mn^{2+}. Strikingly, 64% of the homozygous *atp13a2* mutants showed large apoptotic areas throughout the central nervous system (brain and dorsal spine) after exposure to Mn^{2+}, a phenotype that did not develop in the great majority of the WT control larvae in that same condition (Fig. 4D and E). As for the yeast *ypk9*Δ model, these observations show that *atp13a2* deficiency renders zebrafish larvae much more sensitive to manganese exposure, with the interesting additional information from the zebrafish model that this sensitivity seems to be particularly pronounced in nerve cells in vertebrates.

Given the strong zinc sensitivity phenotype observed in the yeast model, we also tested the effect of zinc exposure on zebrafish larvae. At lower concentrations of Zn^{2+} (up to 0.3 mM), we could not observe any dysmorphology or changes in locomotor behaviour in either control or homozygous *atp13a2* mutant larvae (data not shown). However, at 1 mM $ZnCl_2$, we observed higher lethality and strong tissue damage (often starting in the caudal region) in both the control and mutant larvae (Supplementary Fig. 6). As it was very difficult to detect significant differences between control and *atp13a2* mutant larvae in this condition, we decided to focus on the manganese sensitivity phenotype of the *atp13a2* mutant zebrafish model for the rest of this study.

atp13a2 zebrafish morphants phenocopy *atp13a2* knockout mutants

In a previous study, transient downregulation of *atp13a2* by microinjection of an exon1-intron1 splice-blocking morpholino antisense oligonucleotide (e1i1-MO) was reported to be lethal in zebrafish larvae (Lopes da Fonseca *et al.*, 2013). This suggested that compensatory mechanisms (not induced in the *atp13a2* knockdown larvae) may explain the absence of an overt phenotype (under control conditions) of our *atp13a2* knockout mutants. Another explanation for the apparently contradictory results could be a gene-independent toxicity of the e1i1-MO used previously and we started testing this MO by injection into our *atp13a2*$^{sa18624-/-}$ and *atp13a2*$^{sa14250-/-}$ mutant embryos. At 3 dpf, all embryos were dysmorphic and showed locomotor impairments. In contrast, homozygous mutants injected with a control morpholino did not display any abnormality, indeed suggesting a possible *atp13a2* independent effect elicited by the e1i1-MO (Supplementary Fig. 7). Therefore, for validation of the Mn^{2+} phenotype in *atp13a2* morphants (as

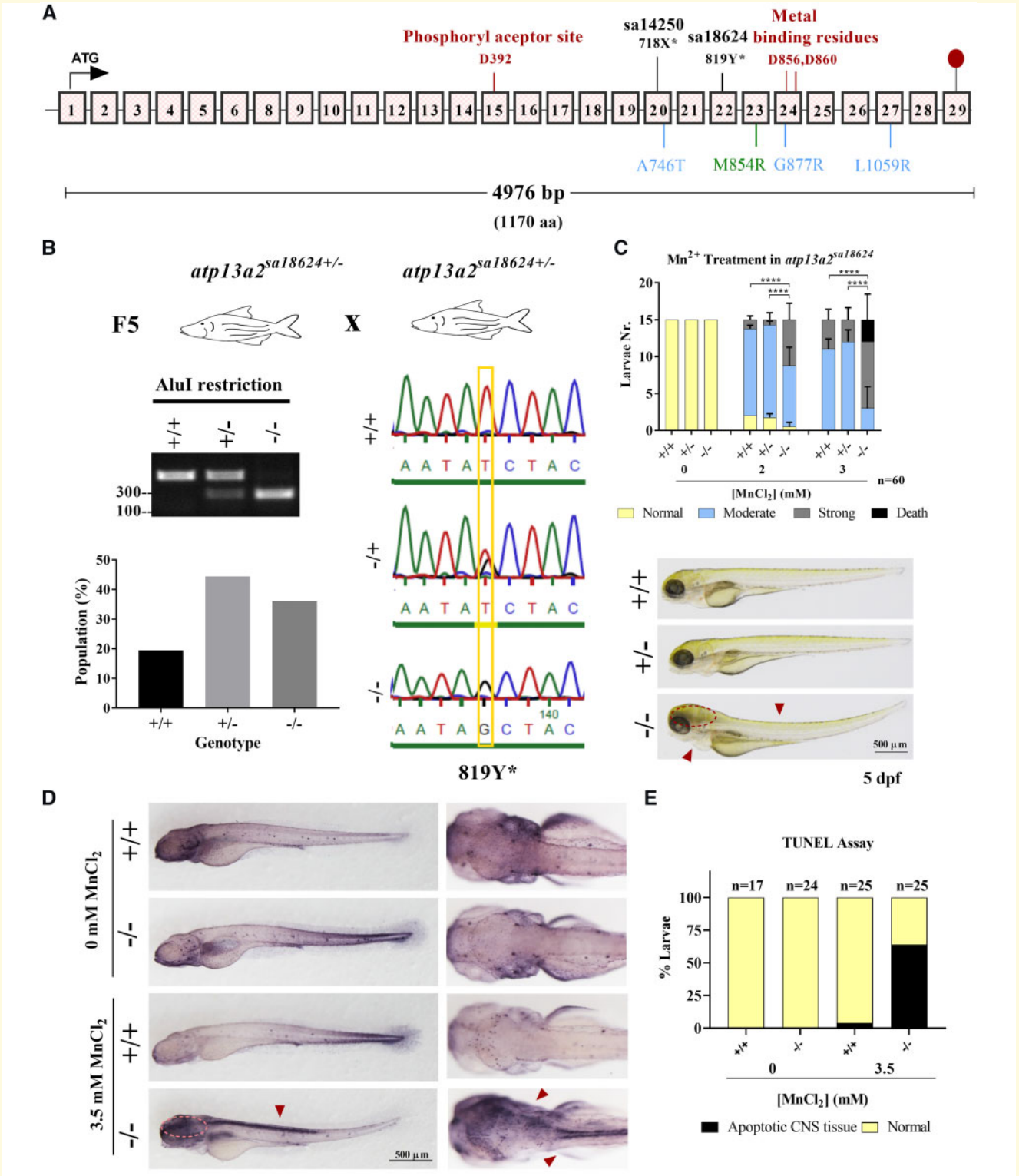

Figure 4 Genotyping and phenotyping of *atp13a2*$^{-/-}$ zebrafish mutants. (**A**) Schematic illustration of the zebrafish *atp13a2* gene structure. Exons are represented as numbered boxes and homologous positions of human disease-associated mutations that are close to mutations present in the zebrafish mutant lines used in this study are indicated (in black, non-sense mutations in zebrafish mutant lines; in blue, KRS-associated mutations; in green, NCL-associated mutation). In red, important domains for the ATP13A2 function are also indicated. (**B**) *atp13a2*$^{sa18624-/+}$ heterozygous carriers were crossed and the offspring was raised to adulthood. AluI restriction analysis showed that 35% of the F6 population were homozygous mutants. Genomic DNA sequencing confirmed the expected mutations in heterozygous and homozygous zebrafish. (**C**) 2 dpf *atp13a2*$^{sa18624+/+}$, *atp13a2*$^{sa18624-/+}$ and *atp13a2*$^{sa18624-/-}$ larvae were incubated without or with 2 and 3 mM $MnCl_2$ for 3 days. All 5 dpf larvae incubated in the presence of $MnCl_2$ lacked the swimming bladder (moderate phenotype), but homozygous *atp13a2*$^{sa18624-/-}$ larvae, in addition, showed increased occurrence of pericardial oedemas, spine curvature, darkening of the brain tissue (strong

opposed to mutants), we designed a translation (ATG-MO) and a different splice-blocking (e2i2-MO) morpholino to inhibit the expression and processing of newly synthesized *atp13a2* mRNA, respectively (Supplementary Fig. 8A). No obvious phenotypes were observed up to 5 dpf upon injection of 8 ng of either morpholino into WT embryos (Supplementary Fig. 8B). The lack of antibodies against the zebrafish Atp13a2 protein prevented the verification of decreased Atp13a2 levels in the morphants generated by injection of the ATG-MO. However, the efficiency of our splice-blocking morpholino was confirmed at 3 dpf by qPCR and sequencing of cDNA from these morphants provided evidence for aberrant *atp13a2* splicing leading to an early stop codon (Supplementary Fig. 8A).

Subsequently, we incubated *atp13a2* morphant larvae (generated with ATG-MO and e2i2-MO) in the presence of 1 and 3 mM $MnCl_2$ and analysed them morphologically at 5 dpf. *atp13a2* morphants were substantially more sensitive to Mn^{2+} than the control larvae (Supplementary Fig. 8C) and surviving larvae displayed similar phenotypes to those previously described for the *atp13a2* mutant lines (pericardial oedemas, darkening of areas in the brain, spine curvature; Supplementary Fig. 8D). Actually, *atp13a2* morphants showed even higher sensitivity to Mn^{2+} compared with the mutant larvae as exposure to 1 mM Mn^{2+} had a similar impact on the morphants as exposure to 3 mM Mn^{2+} on the mutants. Morphants were generated from the commonly used AB zebrafish strain whereas the mutant lines had been created in the Tüpfel long fin strain. A different genetic background may, therefore, at least partially explain that a partial gene knockdown led to a stronger phenotype than a null mutation. Overall, the results obtained in the *atp13a2* morphants (created with our newly designed MOs) and *atp13a2* knockout models were, however, in good agreement and our observations suggest that functional ATP13A2 protects multicellular organisms against manganese toxicity, but that it is not essential for zebrafish development under standard conditions.

Validation of yeast phenotypic hit compounds in *atp13a2* knockout zebrafish

To further validate the hits obtained in the primary yeast screen in a more complex organism, we proceeded to their *in vivo* testing in our *atp13a2* zebrafish mutant line (except for the industrial chelator TEPA). For each compound class, the maximum tolerated concentration was first determined in WT embryos in the absence of Mn^{2+} and sublethal drug concentrations were then tested for their phenotypic rescue potential (Supplementary Fig. 9A). *atp13a2*$^{sa18624-/+}$ and *atp13a2*$^{sa18624-/-}$ larvae at 2 dpf were incubated in medium containing 3.5 mM $MnCl_2$, followed 24 h later by an exchange for medium containing different concentrations of the drugs (0.1–1000 µM) in addition to $MnCl_2$. Two of the 10 hit compounds tested (NAC and FTD) protected dose-dependently against Mn^{2+} toxicity, with an apparently more pronounced effect in mutant than in control larvae (5 dpf). Considering, for instance, the highest drug concentration tested (1 mM), >80% of the *atp13a2* mutant larvae presented merely a moderate phenotype (absence of the swimming bladder) whereas >65% of these larvae either died or presented severe morphological abnormalities in the absence of drug (Fig. 5B and C). NAC and FTD also protected against Mn^{2+} toxicity in the WT larvae, but their relative effect was less pronounced in these animals given a weaker phenotypic impact of Mn^{2+} in the absence of the drug. The remaining drugs tested failed to rescue the phenotype induced by manganese exposure, be it in the WT or mutant larvae (Supplementary Fig. 9B).

Discussion

ATP13A2 and heavy metal stress response in budding yeast and zebrafish

In this study, of around 200 growth conditions tested for *ATP13A2* deficient yeast models in two different genetic backgrounds, only the presence of Mn^{2+}, Co^{2+}, Zn^{2+} and Ni^{2+} led to significant growth impairments in both *ypk9*Δ strains. We also found that, under Zn^{2+}-repletion conditions, post-mitotic *ypk9*Δ cells contained considerably higher concentrations of this ion than WT cells. Accordingly, human cells derived from the olfactory mucosa (hONs) of *ATP13A2*$^{-/-}$ patients showed decreased viability in the presence of Zn^{2+} (Kong *et al.*, 2014; Park *et al.*, 2014). Also, patient cells showed higher intracellular Zn^{2+} levels than control cells only when challenged with $ZnCl_2$. Interestingly, vesicular zinc levels were, however, lower in the *ATP13A2* deficient cells (Kong *et al.*, 2014; Park *et al.*, 2014). Together with our data, all studies indicate that ATP13A2 is critically involved in zinc compartmentalization or externalization under conditions where

phenotype; see arrows) and lethality. Data shown are means ± SDs for 60 larvae incubated and phenotyped in four separate wells (15 larvae per well). A likelihood ratio test was applied to verify the statistical significance of the phenotypic differences between WT (and heterozygous) larvae and homozygous *atp13a2* larvae (****$P < 0.0001$). (**D**) A TUNEL assay was used to detect apoptotic cells in 5 dpf larvae exposed or not to $MnCl_2$ as described under **B**. (**E**) Quantification of the larvae with extensive apoptotic areas in the CNS (indicated with a dotted circle and red arrowheads in **D**) as based on the TUNEL assay.

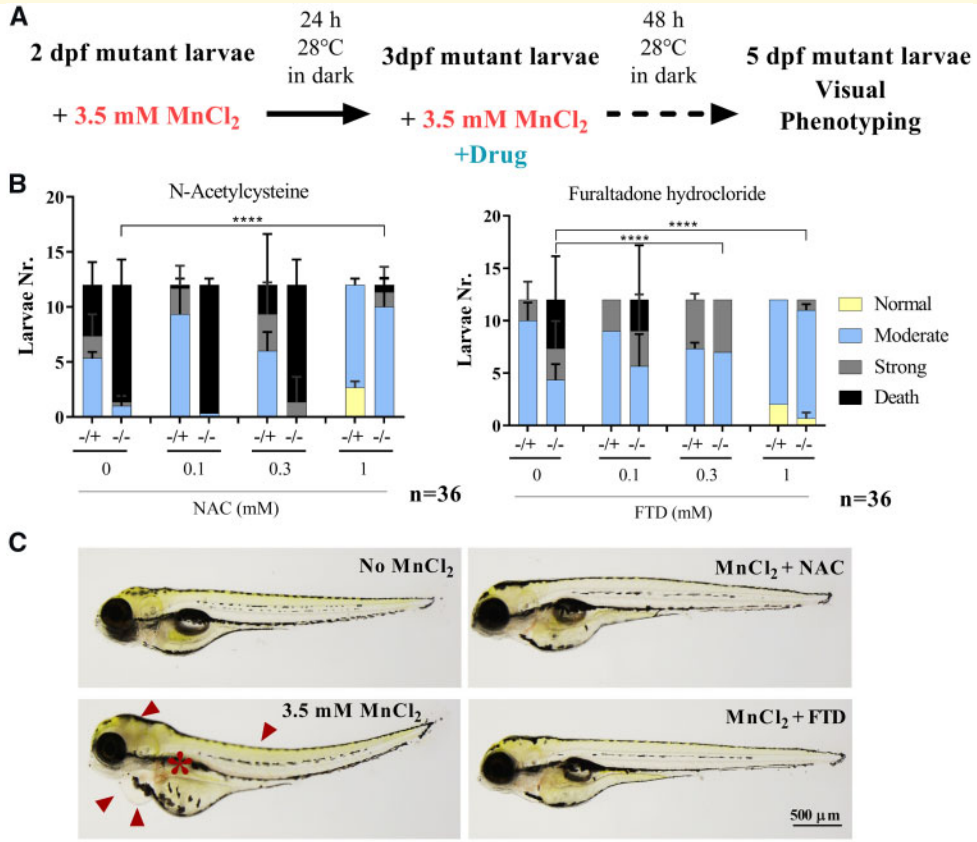

Figure 5 Secondary drug screening in *atp13a2*$^{sa18624-/-}$ zebrafish larvae. (**A**) Schematic representation of the drug-screening methodology. Two dpf larvae were incubated with 3.5 mM $MnCl_2$. After 24 h, media was replaced by new media containing 0.1, 0.3 and 1 mM of each tested drug in addition to $MnCl_2$. At 5 dpf, the phenotype was visually scored for each animal. (**B**) Of the 10 drugs tested in zebrafish larvae, NAC and FTD showed a protective effect against Mn^{2+} toxicity. Data shown are means ± SDs for 36 larvae incubated and phenotyped in three separate wells (12 larvae per well). A likelihood ratio test was applied to verify the statistical significance of the phenotypic differences observed between homozygous *atp13a2* larvae treated or not with the drug hit compounds (****$P < 0.0001$). (**C**) Representative images of *atp13a2*$^{sa18624-/-}$ larvae at 5 dpf. In the absence of $MnCl_2$, mutant larvae showed a normal development, whereas treatment with 3.5 mM $MnCl_2$ led to a severe phenotype featuring pericardial oedemas, spine curvature and darkening of the brain region (arrowheads) in addition to the absence of the swimming bladder (*). This phenotype was clearly ameliorated by treatment with 1 mM NAC or FTD.

storage compartments (vacuole/lysosomes) become overloaded. Further supporting the involvement of ATP13A2 in metal detoxification, we observed that deletion or transient knockdown of *atp13a2* in zebrafish caused increased sensitivity to $MnCl_2$ exposure, resulting in pericardial oedemas, spine curvature and higher mortality. As in the yeast model, we could only observe an obvious phenotype in zebrafish when we challenged the model with relatively high metal ion concentrations.

The main goal of this study was to perform a drug screen for *ATP13A2* deficiencies, calling for acute exposure protocols yielding relevant phenotypes in a short time frame to allow for HTP screening. We did not evaluate long-term exposure to heavy metals, but considering that *ATP13A2* deficiencies are linked to juvenile and adult rare neurodegenerative disorders, it might be that a slight dysregulation of heavy metal homeostasis leads to gradual accumulation and/or mis-localization of those metals over the years until the onset of disease symptoms. Heavy metals have been found to be part of lipofuscins, a hallmark of NCLs, as well as of abnormal aggregates containing mainly α-synuclein in the brain of Parkinson's disease patients (Terman and Brunk, 1998; Gardner *et al.*, 2017). The fact that these features have also been observed in *ATP13A2*-deficient patients and animal models, combined with ample evidence for the role of ATP13A2 in heavy metal homeostasis, suggest that heavy metals may play a pivotal role in the pathology of *ATP13A2*-associated disorders. Notably, the clinical heterogeneity observed in ATP13A2 patients may result from varying interactions between environmental metal exposures and genetic factors (Rentschler *et al.*, 2012).

Primary and secondary drug screen for *ATP13A2* deficiencies

In the present study, we developed and combined two phenotypic drug-screening assays, using budding yeast

and zebrafish to identify drugs that could be used to treat *ATP13A2*-associated disorders. Currently, 32 pathogenic mutations have been described for *ATP13A2* and most of these mutations appear to cause protein instability or functional disruption (Ramirez *et al.*, 2006; Podhajska *et al.*, 2012; Estrada-Cuzcano *et al.*, 2017). We, therefore, opted for complete loss-of-function models, seeking to identify drugs with therapeutic potential for most of these disorders.

As the mechanism of action of ATP13A2 in heavy metal detoxification seems to be well-conserved (Gitler *et al.*, 2009; Schmidt *et al.*, 2009; Tan *et al.*, 2011; Kong *et al.*, 2014; Park *et al.*, 2014), we used yeast as a HTP screening platform for chemicals that alleviate Zn^{2+}-induced stress in *YPK9* deleted cells. We focused the screen on libraries containing in large part FDA- and EMA-approved drugs and tested in total 2553 chemical compounds. From the primary screening, 11 hits were validated in a concentration-response assay. For further validation of the hits, an *in vivo* disease model in zebrafish was established using *atp13a2* mutant larvae exposed to Mn^{2+}. In addition to this *in vivo* evaluation of compound efficacy, zebrafish larvae allow to concomitantly address drug safety and drug delivery through the blood-brain barrier, which is a major challenge in drug discovery for neurodegenerative disorders (Eliceiri *et al.*, 2011; Kanungo *et al.*, 2014; Zeng *et al.*, 2017).

Of the 11 hits identified in the yeast-based primary screen, NAC and FTD were validated as being able to alleviate Mn^{2+} toxicity in the zebrafish-based secondary screen. NAC was initially prescribed for the treatment of paracetamol-induced hepatoxicity by restoring hepatic concentrations of glutathione and also as a mucolytic agent (Bavarsad Shahripour *et al.*, 2014). However, in the last year, several studies have reported a neuroprotective function for NAC by increasing the glutathione levels (Bavarsad Shahripour *et al.*, 2014). Furthermore, glutathione deficiency has long been implicated in the development of Parkinson's disease (Perry *et al.*, 1982; Bjorklund *et al.*, 2018). In fact, one ongoing clinical trial using NAC has been reported for Parkinson's disease (Monti *et al.*, 2015) and NAC treatment also seems to be beneficial for Alzheimer's disease where it showed positive effects on some secondary outcome measures (cognitive tests; Adair *et al.*, 2001). Interestingly, independently to this study, it has been reported that NAC mitigates Zn^{2+}- and Fe^{2+}-induced toxicity in *ATP13A2*$^{-/-}$ hONs and CHO cells (Park *et al.*, 2014; Rinaldi *et al.*, 2015). The positive effects of NAC in three different disease models for *ATP13A2* deficiency, in addition to the described beneficial effects in Parkinson's and Alzheimer's disease, suggest that its nutritional supplementation could be of therapeutic value in *ATP13A2*-associated disorders. Interestingly, another mucolytic agent, Ambroxol, has emerged recently as a drug with beneficial effects in Parkinson's disease and Gaucher's disease. Not only does Ambroxol seem to be a potent chaperone for glucocerebrosidase, the enzyme deficient in Gaucher patients, but it has been shown to promote exocytosis, as well as lysosomal and mitochondrial biogenesis (Magalhaes *et al.*, 2018). It remains to be explored whether the beneficial effects of NAC in neurodegenerative disorders may be mediated at least in part through similar properties.

In contrast, little is known about FTD, a nitrofuran antibiotic primarily used for bacterial infections in poultry (Nouws *et al.*, 1987). Currently, nitrofurans are prohibited in the EU for livestock production due to their potential carcinogenicity. However, nitrofuran antibiotics can still be used in humans for the treatment of infections of the urinary tract and the skin as well as bacterial diarrhoea (Guay, 2008; Vasheghani *et al.*, 2008). Interestingly, although five members of this family of antibiotics were present in one of the libraries screened in this study, only FTD was identified as a hit. In comparison to other nitrofurans, FTD has an additional morpholinomethyl modification, which is retained in FTD-derived metabolites (AMOZ; Supplementary Fig. 10; Vass *et al.*, 2008). In the zinquin chelation assay, FTD exhibited a slight chelation activity at high concentrations, suggesting that intracellular metal ion chelation by FTD and/or one or several of its biotransformation product(s) could be a mechanism of action. Although the use of FTD is currently controversial, our study suggests that this compound possesses some favourable features in the context of heavy metal exposure, more particularly in combination with *ATP13A2* deficiency, and that it could be used for chemical lead optimization.

Chelating agents have been proposed as effective secondary antioxidants by stabilizing the oxidative form of heavy metals and thereby decreasing metal ion induced oxidative stress that may, for instance, cause cell death (Turan *et al.*, 2016). Moreover, KRS belongs to the group of neurodegenerative disorders with brain iron accumulation and several *ATP13A2* deficiency models, including the yeast and zebrafish models used here, strongly implicate this protein in the compartmentalization and externalization of heavy metals. Taken together, these findings suggest that chelation therapy could be beneficial for the treatment of *ATP13A2*-associated disorders. Some clinical studies already support the therapeutic use of chelators for other neurodegenerative disorders, such as Friedreich's ataxia (Boddaert *et al.*, 2007; Dusek *et al.*, 2016; Martin-Bastida *et al.*, 2017). In this disease, the decrease of iron–sulphur clusters and haem formation cause iron accumulation in mitochondria, and administration of deferiprone to these patients over a 6-month period reduced iron content, resulting in improved clinical symptoms (Boddaert *et al.*, 2007). However, larger clinical trials and studies are still needed, as chelation therapy remains controversial; important metals needed for normal cellular function could be unspecifically chelated, resulting in non-desired side effects (Nunez and Chana-Cuevas, 2018).

Most drugs identified in the yeast model failed to rescue the phenotype in the zebrafish model. Possible reasons for this could be: (i) a low penetration through the blood-brain barrier, (ii) a yeast-specific mechanism of action and/or (iii) a Zn^{2+}-specific effect. Indeed, cephalosporin antibiotics are known to have a generally poor blood-brain barrier penetration (Lutsar and Friedland, 2000). Our finding that all cephalosporin antibiotics (belonging to the class of β-lactam antibiotics) contained in the Prestwick library were identified as hits in the yeast-based primary screen is nevertheless noteworthy. It has been demonstrated that β-lactams confer neuroprotection by decreasing synaptic glutamate levels through the increase of glutamate uptake in the cells. This effect was shown to be beneficial in an SOD1-G93A transgenic mouse model of amyotrophic lateral sclerosis (Rothstein *et al.*, 2005), a disease that has also been recently linked to *ATP13A2*-deficiency (Spataro *et al.*, 2019). In the mouse model, ceftriaxone (a third-generation β-lactam not contained in the chemical libraries screened in this study) treatment delayed the loss of muscle strength and body weight. In addition, β-lactams are also known as metal chelators such as Zn^{2+}, Cu^{2+}, Co^{2+}, Ni^{2+} (Mukherjee and Ghosh, 1995), although they did not show a high affinity for Zn^{2+} using our zinquin assay.

Other interesting hits were VU152100 and VU10010, two selective activators of the M4 muscarinic acetylcholine receptor, which were able to rescue the yeast phenotype in the micromolar range. M4 receptors are G protein-coupled receptors that play an important role in regulating midbrain dopaminergic activity; they are attractive entry points for the treatment of disorders involving altered dopaminergic function in the basal ganglia, including Parkinson's disease (Brady *et al.*, 2008). However, the yeast genome does not encode any protein with appreciable homology to the human M4 receptor. Similarly, two additional non-approved drugs identified as hits in the yeast screen, AMG9810 and ML365, bind to proteins (vanilloid TRPV1 receptor and TASK-1 channel, respectively; Gavva *et al.*, 2005; Zou *et al.*, 2010) that are not conserved in yeast. Understanding the mechanism by which these drugs alleviate the Zn^{2+} toxicity in the yeast *ypk9*Δ mutant thus requires further investigation.

The cellular protectant properties of the hits identified during our primary HTP screen demonstrate the strength of yeast for the identification of chemical suppressors of *ATP13A2*-associated disease phenotypes. However, *in vivo* secondary screening is clearly important for validating the bioactivity of the 'primary' hits in the context of a multicellular organism. In this study, we utilized the advantages of yeast and zebrafish *ATP13A2* deficiency models, combining these two bioassay systems to create an integrated screening platform for drug repurposing. Ultimately, this platform might accelerate both the repurposing of existing drugs, as well as the discovery of new lead compounds for the treatment of neurodegenerative disorders associated with the dysregulation of heavy metal homeostasis. As a next step, both NAC and FTD, as well as some of the other hits with activity only in the yeast model, should be tested in other *in vivo* models of *ATP13A2* deficiency, such as mouse or dog (Farias *et al.*, 2011; Schultheis *et al.*, 2013).

Supplementary material

Supplementary material is available at *Brain Communications* online.

Acknowledgements

We thank the Clinical & Experimental Neuroscience group of LCSB and Semra Smajic for their help with performing automated and HTP procedures during the primary drug screening. The automated screening platform was funded through a PEARL grant of the Luxembourg National Research Fund (FNR) to Rejko Krüger. In addition, we want to thank Enrico Glaab and Todor Kondic for their help with statistical analyses, and Ibrahim Boussaad and Gerald Cruciani for their critical comments throughout the development of the project. We thank Cédric Guignard and Johanna Ziebel (LIST) for performing the inductively coupled plasma—mass spectrometry metal measurements in yeast cells. Finally, we are also grateful to the LCSB fish caretaker team for their valuable daily work.

Funding

This work was supported in part by donations from the ATOZ foundation, Mr. Norbert Becker and by a Pelican award from the Fondation du Pélican de Mie et Pierre Hippert-Faber to UHM. The inductively coupled plasma—mass spectrometry measurements were partially financed by a 2018 Biomedicine award to UHM of the Doctoral School in Systems and Molecular Biomedicine at the University of Luxembourg.

Competing interests

The authors report no competing interests.

References

Adair JC, Knoefel JE, Morgan N. Controlled trial of N-acetylcysteine for patients with probable Alzheimer's disease. Neurology 2001; 57: 1515–7.

Alberti S, Gitler AD, Lindquist S. A suite of Gateway cloning vectors for high-throughput genetic analysis in *Saccharomyces cerevisiae*. Yeast 2007; 24: 913–9.

Bakthavatsalam S, Das Sharma S, Sonawane M, Thirumalai V, Datta A. A zebrafish model of manganism reveals reversible and treatable

symptoms that are independent of neurotoxicity. Dis Model Mech 2014; 7: 1239–51.
Bavarsad Shahripour R, Harrigan MR, Alexandrov AV. N-acetylcysteine (NAC) in neurological disorders: mechanisms of action and therapeutic opportunities. Brain Behav 2014; 4: 108–22.
Behrens MI, Bruggemann N, Chana P, Venegas P, Kagi M, Parrao T, et al. Clinical spectrum of Kufor-Rakeb syndrome in the Chilean kindred with ATP13A2 mutations. Mov Disord 2010; 25: 1929–37.
Bjorklund G, Stejskal V, Urbina MA, Dadar M, Chirumbolo S, Mutter J. Metals and Parkinson's disease: mechanisms and biochemical processes. Curr Med Chem 2018; 25: 2198–214.
Boddaert N, Le Quan Sang KH, Rotig A, Leroy-Willig A, Gallet S, Brunelle F, et al. Selective iron chelation in Friedreich ataxia: biologic and clinical implications. Blood 2007; 110: 401–8.
Brachmann CB, Davies A, Cost GJ, Caputo E, Li J, Hieter P, Boeke JD. Designer deletion strains derived from *Saccharomyces cerevisiae* S288C: a useful set of strains and plasmids for PCR-mediated gene disruption and other applications. Yeast 1998; 14: 115–32.
Brady AE, Jones CK, Bridges TM, Kennedy JP, Thompson AD, Heiman JU, et al. Centrally active allosteric potentiators of the M4 muscarinic acetylcholine receptor reverse amphetamine-induced hyperlocomotor activity in rats. J Pharmacol Exp Ther 2008; 327: 941–53.
Bras J, Verloes A, Schneider SA, Mole SE, Guerreiro RJ. Mutation of the parkinsonism gene ATP13A2 causes neuronal ceroid-lipofuscinosis. Hum Mol Genet 2012; 21: 2646–50.
Cicero CE, Mostile G, Vasta R, Rapisarda V, Signorelli SS, Ferrante M, et al. Metals and neurodegenerative diseases. A systematic review. Environ Res 2017; 159: 82–94.
Cotticelli MG, Rasmussen L, Kushner NL, McKellip S, Sosa MI, Manouvakhova A, et al. Primary and secondary drug screening assays for Friedreich ataxia. J Biomol Screen 2012; 17: 303–13.
Dehay B, Ramirez A, Martinez-Vicente M, Perier C, Canron MH, Doudnikoff E, et al. Loss of P-type ATPase ATP13A2/PARK9 function induces general lysosomal deficiency and leads to Parkinson disease neurodegeneration. Proc Natl Acad Sci USA 2012; 109: 9611–6.
Dusek P, Schneider SA, Aaseth J. Iron chelation in the treatment of neurodegenerative diseases. J Trace Elem Med Biol 2016; 38: 81–92.
Eliceiri BP, Gonzalez AM, Baird A. Zebrafish model of the blood-brain barrier: morphological and permeability studies. Methods Mol Biol 2011; 686: 371–8.
Estrada-Cuzcano A, Martin S, Chamova T, Synofzik M, Timmann D, Holemans T, et al. Loss-of-function mutations in the ATP13A2/PARK9 gene cause complicated hereditary spastic paraplegia (SPG78). Brain 2017; 140: 287–305.
Farias FH, Zeng R, Johnson GS, Wininger FA, Taylor JF, Schnabel RD, et al. A truncating mutation in ATP13A2 is responsible for adult-onset neuronal ceroid lipofuscinosis in Tibetan terriers. Neurobiol Dis 2011; 42: 468–74.
Gardner B, Dieriks BV, Cameron S, Mendis LHS, Turner C, Faull RLM, et al. Metal concentrations and distributions in the human olfactory bulb in Parkinson's disease. Sci Rep 2017; 7: 10454.
Gavva NR, Tamir R, Qu Y, Klionsky L, Zhang TJ, Immke D, et al. AMG 9810 [(E)-3-(4-t-butylphenyl)-N-(2,3-dihydrobenzo[b][1,4] dioxin-6-yl)acrylamide], a novel vanilloid receptor 1 (TRPV1) antagonist with antihyperalgesic properties. J Pharmacol Exp Ther 2005; 313: 474–84.
Gietz RD, Woods RA. Transformation of yeast by lithium acetate/single-stranded carrier DNA/polyethylene glycol method. Methods Enzymol 2002; 350: 87–96.
Gitler AD, Chesi A, Geddie ML, Strathearn KE, Hamamichi S, Hill KJ, et al. Alpha-synuclein is part of a diverse and highly conserved interaction network that includes PARK9 and manganese toxicity. Nat Genet 2009; 41: 308–15.
Grubman A, Pollari E, Duncan C, Caragounis A, Blom T, Volitakis I, et al. Deregulation of biometal homeostasis: the missing link for neuronal ceroid lipofuscinoses? Metallomics 2014; 6: 932–43.
Grunewald A, Arns B, Seibler P, Rakovic A, Munchau A, Ramirez A, et al. ATP13A2 mutations impair mitochondrial function in fibroblasts from patients with Kufor-Rakeb syndrome. Neurobiol Aging 2012; 33: 1843.e1–7.
Guay DR. Contemporary management of uncomplicated urinary tract infections. Drugs 2008; 68: 1169–205.
Howe K, Clark MD, Torroja CF, Torrance J, Berthelot C, Muffato M, et al. The zebrafish reference genome sequence and its relationship to the human genome. Nature 2013; 496: 498–503.
Jung PP, Christian N, Kay DP, Skupin A, Linster CL. Protocols and programs for high-throughput growth and aging phenotyping in yeast. PLoS One 2015; 10: e0119807.
Kanungo J, Cuevas E, Ali SF, Paule MG. Zebrafish model in drug safety assessment. Curr Pharm Des 2014; 20: 5416–29.
Kara E, Tucci A, Manzoni C, Lynch DS, Elpidorou M, Bettencourt C, et al. Genetic and phenotypic characterization of complex hereditary spastic paraplegia. Brain 2016; 139: 1904–18.
Kett LR, Stiller B, Bernath MM, Tasset I, Blesa J, Jackson-Lewis V, et al. alpha-Synuclein-independent histopathological and motor deficits in mice lacking the endolysosomal Parkinsonism protein Atp13a2. J Neurosci 2015; 35: 5724–42.
Kong SM, Chan BK, Park JS, Hill KJ, Aitken JB, Cottle L, et al. Parkinson's disease-linked human PARK9/ATP13A2 maintains zinc homeostasis and promotes alpha-Synuclein externalization via exosomes. Hum Mol Genet 2014; 23: 2816–33.
Livak KJ, Schmittgen TD. Analysis of relative gene expression data using real-time quantitative PCR and the 2(-Delta Delta C(T)) method. Methods 2001; 25: 402–8.
Lopes da Fonseca T, Correia A, Hasselaar W, van der Linde HC, Willemsen R, Outeiro TF. The zebrafish homologue of Parkinson's disease ATP13A2 is essential for embryonic survival. Brain Res Bull 2013; 90: 118–26.
Lutsar I, Friedland IR. Pharmacokinetics and pharmacodynamics of cephalosporins in cerebrospinal fluid. Clin Pharmacokinet 2000; 39: 335–43.
Magalhaes J, Gegg ME, Migdalska-Richards A, Schapira AH. Effects of ambroxol on the autophagy-lysosome pathway and mitochondria in primary cortical neurons. Sci Rep 2018; 8: 1385.
Martin-Bastida A, Ward RJ, Newbould R, Piccini P, Sharp D, Kabba C, et al. Brain iron chelation by deferiprone in a phase 2 randomised double-blinded placebo controlled clinical trial in Parkinson's disease. Sci Rep 2017; 7: 1398.
McCurley AT, Callard GV. Characterization of housekeeping genes in zebrafish: male-female differences and effects of tissue type, developmental stage and chemical treatment. BMC Mol Biol 2008; 9: 102.
Monti DA, Newberg AB, Kremens D, 2015. Physiological Effects of Nutritional Support in Patients with Parkinson's Disease. *Clinicaltrialsgov*. Available from: https://clinicaltrials.gov/ct2/show/study/NCT02445651 (10 April 2019, date last accessed).
Mukherjee G, Ghosh T. Metal ion interaction with penicillins–Part VII: mixed-ligand complex formation of cobalt(II), nickel(II), copper(II), and Zinc(II) with ampicillin and nucleic bases. J Inorg Biochem 1995; 59: 827–33.
Nouws JF, Vree TB, Aerts MM, Degen M, Driessens F. Some pharmacokinetic data about furaltadone and nitrofurazone administered orally to preruminant calves. Vet Q 1987; 9: 208–14.
Nunez MT, Chana-Cuevas P. New perspectives in iron chelation therapy for the treatment of neurodegenerative diseases. Pharmaceuticals (Basel) 2018; 11: 109.
Palmer DN, Fearnley IM, Walker JE, Hall NA, Lake BD, Wolfe LS, et al. Mitochondrial ATP synthase subunit c storage in the ceroid-lipofuscinoses (Batten disease). Am J Med Genet 1992; 42: 561–7.
Park JS, Koentjoro B, Veivers D, Mackay-Sim A, Sue CM. Parkinson's disease-associated human ATP13A2 (PARK9) deficiency causes zinc

dyshomeostasis and mitochondrial dysfunction. Hum Mol Genet 2014; 23: 2802–15.
Perry TL, Godin DV, Hansen S. Parkinson's disease: a disorder due to nigral glutathione deficiency? Neurosci Lett 1982; 33: 305–10.
Podhajska A, Musso A, Trancikova A, Stafa K, Moser R, Sonnay S, et al. Common pathogenic effects of missense mutations in the P-type ATPase ATP13A2 (PARK9) associated with early-onset parkinsonism. PLoS One 2012; 7: e39942.
Ramirez A, Heimbach A, Grundemann J, Stiller B, Hampshire D, Cid LP, et al. Hereditary parkinsonism with dementia is caused by mutations in ATP13A2, encoding a lysosomal type 5 P-type ATPase. Nat Genet 2006; 38: 1184–91.
Rentschler G, Covolo L, Haddad AA, Lucchini RG, Zoni S, Broberg K. ATP13A2 (PARK9) polymorphisms influence the neurotoxic effects of manganese. Neurotoxicology 2012; 33: 697–702.
Rinaldi DE, Corradi GR, Cuesta LM, Adamo HP, de Tezanos Pinto F. The Parkinson-associated human P5B-ATPase ATP13A2 protects against the iron-induced cytotoxicity. Biochim Biophys Acta 2015; 1848: 1646–55.
Rogers B, Decottignies A, Kolaczkowski M, Carvajal E, Balzi E, Goffeau A. The pleitropic drug ABC transporters from *Saccharomyces cerevisiae*. J Mol Microbiol Biotechnol 2001; 3: 207–14.
Rosen JN, Sweeney MF, Mably JD. Microinjection of zebrafish embryos to analyze gene function. J Vis Exp 2009; (25): e1115. doi: 10.3791/1115.
Roth JA. Correlation between the biochemical pathways altered by mutated Parkinson-related genes and chronic exposure to manganese. Neurotoxicology 2014; 44: 314–25.
Rothstein JD, Patel S, Regan MR, Haenggeli C, Huang YH, Bergles DE, et al. Beta-lactam antibiotics offer neuroprotection by increasing glutamate transporter expression. Nature 2005; 433: 73–7.
Schmidt K, Wolfe DM, Stiller B, Pearce DA. Cd2+, Mn2+, Ni2+ and Se2+ toxicity to *Saccharomyces cerevisiae* lacking YPK9p the orthologue of human ATP13A2. Biochem Biophys Res Commun 2009; 383: 198–202.
Schneider SA, Paisan-Ruiz C, Quinn NP, Lees AJ, Houlden H, Hardy J, et al. ATP13A2 mutations (PARK9) cause neurodegeneration with brain iron accumulation. Mov Disord 2010; 25: 979–84.
Schultheis PJ, Fleming SM, Clippinger AK, Lewis J, Tsunemi T, Giasson B, et al. Atp13a2-deficient mice exhibit neuronal ceroid lipofuscinosis, limited alpha-synuclein accumulation and age-dependent sensorimotor deficits. Hum Mol Genet 2013; 22: 2067–82.
Schultheis PJ, Hagen TT, O'Toole KK, Tachibana A, Burke CR, McGill DL, et al. Characterization of the P5 subfamily of P-type transport ATPases in mice. Biochem Biophys Res Commun 2004; 323: 731–8.
Soma S, Latimer AJ, Chun H, Vicary AC, Timbalia SA, Boulet A, et al. Elesclomol restores mitochondrial function in genetic models of copper deficiency. Proc Natl Acad Sci USA 2018; 115: 8161–6.
Sorensen DM, Buch-Pedersen MJ, Palmgren MG. Structural divergence between the two subgroups of P5 ATPases. Biochim Biophys Acta 2010; 1797: 846–55.
Spataro R, Kousi M, Farhan SMK, Willer JR, Ross JP, Dion PA, et al. Mutations in ATP13A2 (PARK9) are associated with an amyotrophic lateral sclerosis-like phenotype, implicating this locus in further phenotypic expansion. Hum Genomics 2019; 13: 19.
Tan J, Zhang T, Jiang L, Chi J, Hu D, Pan Q, et al. Regulation of intracellular manganese homeostasis by Kufor-Rakeb syndrome-associated ATP13A2 protein. J Biol Chem 2011; 286: 29654–62.
Tardiff DF, Jui NT, Khurana V, Tambe MA, Thompson ML, Chung CY, et al. Yeast reveal a "druggable" Rsp5/Nedd4 network that ameliorates alpha-synuclein toxicity in neurons. Science 2013; 342: 979–83.
Tardiff DF, Tucci ML, Caldwell KA, Caldwell GA, Lindquist S. Different 8-hydroxyquinolines protect models of TDP-43 protein, alpha-synuclein, and polyglutamine proteotoxicity through distinct mechanisms. J Biol Chem 2012; 287: 4107–20.
Terman A, Brunk UT. Lipofuscin: mechanisms of formation and increase with age. APMIS 1998; 106: 265–76.
Turan B, Şendil K, Şengül E, Gültekin MS, Taslimi P, Gulçin İ, et al. The synthesis of some beta-lactams and investigation of their metal-chelating activity, carbonic anhydrase and acetylcholinesterase inhibition profiles. J Enzyme Inhib Med Chem 2016; 31: 79–88.
Usenovic M, Knight AL, Ray A, Wong V, Brown KR, Caldwell GA, et al. Identification of novel ATP13A2 interactors and their role in alpha-synuclein misfolding and toxicity. Hum Mol Genet 2012; 21: 3785–94.
Usenovic M, Tresse E, Mazzulli JR, Taylor JP, Krainc D. Deficiency of ATP13A2 leads to lysosomal dysfunction, alpha-synuclein accumulation, and neurotoxicity. J Neurosci 2012; 32: 4240–6.
van Veen S, Sorensen DM, Holemans T, Holen HW, Palmgren MG, Vangheluwe P. Cellular function and pathological role of ATP13A2 and related P-type transport ATPases in Parkinson's disease and other neurological disorders. Front Mol Neurosci 2014; 7: 48.
Vasheghani MM, Bayat M, Rezaei F, Bayat A, Karimipour M. Effect of low-level laser therapy on mast cells in second-degree burns in rats. Photomed Laser Surg 2008; 26: 1–5.
Vass M, Hruska K, Franek M. Nitrofuran antibiotics: a review on the application, prohibition and residual analysis. Vet Med-Czech 2008; 53: 469–500.
Vincent BM, Tardiff DF, Piotrowski JS, Aron R, Lucas MC, Chung CY, et al. Inhibiting stearoyl-CoA desaturase ameliorates alpha-synuclein cytotoxicity. Cell Rep 2018; 25: 2742–54.e31.
Westerfield M. The zebrafish book. A guide for the laboratory use of zebrafish (Danio rerio). 4th edn. Eugene: University of Oregon Press; 2000.
Wohlke A, Philipp U, Bock P, Beineke A, Lichtner P, Meitinger T, et al. A one base pair deletion in the canine ATP13A2 gene causes exon skipping and late-onset neuronal ceroid lipofuscinosis in the Tibetan terrier. PLoS Genet 2011; 7: e1002304.
Xu H, Li C, Zeng Q, Agrawal I, Zhu X, Gong Z. Genome-wide identification of suitable zebrafish *Danio rerio* reference genes for normalization of gene expression data by RT-qPCR. J Fish Biol 2016; 88: 2095–110.
Zeng A, Ye T, Cao D, Huang X, Yang Y, Chen X, et al. Identify a blood-brain barrier penetrating drug-TNB using zebrafish orthotopic glioblastoma xenograft model. Sci Rep 2017; 7: 14372.
Zou B, Flaherty DP, Simpson DS, Maki BE, Miller MR, Shi J, et al. ML365: development of bis-amides as selective inhibitors of the KCNK3/TASK1 two pore potassium channel. In: Probe reports from the NIH molecular libraries program [Internet]. Bethesda, MD: National Center for Biotechnology Information (US); 2010. Available from: https://www.ncbi.nlm.nih.gov/books/NBK179826/